Studying the Effects of Chemistry and Geometry on DSA Hole-shrink Process in Three Dimensions

Chun Zhou[a], Tsuyoshi Kurosawa[b], Takahiro Dazai[b], Jan Doise[c], Jiaxing Ren[a], Cody Bezik[a], Tamar Segal-Peretz[d], Akiyoshi Yamazaki[b], Roel Gronheid[c], Paulina Rincon-Delgadillo[c], Juan de Pablo[a], Paul F. Nealey[a]

[a]Institute for Molecular Engineering, University of Chicago, 5640 S. Ellis Ave, Chicago, 60637, United States; [b]Tokyo Ohka Kogyo Co., Ltd.1590 Tabata, Samukawa-machi, Koza-gun, Kanagawa-ken 253-0114, Japan; [c]Imec, Kapeldreef 75, B-3001 Leuven, Belgium; [d]Department of Chemical Engineering, Technion-Israel Institute of Technology, Haifa 32000, Israel

ABSTRACT

Acquiring three-dimensional information becomes increasingly important for the development of block copolymer (BCP) directed self-assembly (DSA) lithography, as 2D imaging is no longer sufficient to describe the 3D nature of DSA morphology and probe hidden structures under the surface. In this study, using post-DSA membrane fabrication technique and STEM (scanning transmission electron microscopy) tomography we were able to characterize the 3D structures of BCP in graphoepitaxial DSA hole shrink process. Different DSA structures of singlets formed in templated holes with different surface chemistry and geometry were successfully captured and their 3D shapes were reconstructed from tomography data. The results reveal that strong PS-preferential sidewalls are necessary to create vertical DSA cylinders and that template size outside of process window could result in defective DSA results in three dimensions. Our study as well as the established 3D metrology would greatly help to develop a fundamental understanding of the key DSA factors for optimization of the graphoepitaxial hole shrink process.

Keywords: directed self-assembly; block copolymer; hole shrink; tomography; 3D reconstruction; defectivity

1. INTRODUCTION

Directed self-assembly (DSA) of block copolymers (BCP) has been widely investigated as a potential patterning solution to extend lithography to generate smaller and denser features[1,2]. Graphoepitaxial DSA of cylinder-forming BCP is a promising implementation of DSA to fabricate uniform holes well below the conventional lithography resolution.[3] In a typical DSA hole shrink process, the guide holes matching the BCP size are firstly made using conventional lithographic method. Then, a cylinder forming polystyrene-block-poly(methyl methacrylate) (PS-*b*-PMMA) is spin-coated and phase separated in the confined space. During annealing, vertical PMMA cylindrical domains are formed in the center of the hole guide patterns. After selectively removing PMMA block, the shrinkage of hole pattern dimensions depending on the molecular weight of PS-b-PMMA is achieved.[3,4]

Currently, most studies are evaluating the DSA hole shrink process based on observations from 2D top view images obtained from scanning electron microscopes (SEM), like statistical study of process window[5], in which case the insight of three-dimensional BCP morphologies inside the holes are limited. Judging from top view images solely could result in the misinterpretations when analyzing the defectively of DSA hole shrink process because the defects might be hidden under the surface.[6] Although some simulation studies have predicted that the three-dimensional DSA structure is affected by factors including the size of guide holes, the compositions of BCP and the affinity of surface[7–9], it is often difficult to evaluate the accuracy of these simulation results due to the lack of direct comparison from experimental results.[6] Therefore, it is very valuable to obtain precise 3D information of BCP assembled inside the holes.

Here, we developed a non-destructive 3D metrology for graphepitaxial hole shrink process using post-DSA membrane fabrication techniques and STEM tomography[10,11]. The self-assembly of PS-*b*-PMMA cylinders were directed by guide holes made of spin-on carbon (SOC) and spin-on glass (SOG) on silicon nitride coated substrate, which was then made

into membrane sample for TEM characterization. Two different brush was used to modify the affinity of sidewall and bottom surface separately and study the effect of surface modification on confined cylinder morphology. By comparing the tomography results with simulated morphologies, we were able to predict which surface conditions would result in defective DSA structure. A similar 3D metrology was applied to 300 mm track-processed wafer and the 3D structures of singlets with different template size were reconstructed from tomography series. Different defective morphologies happening outside of the process window were probed.

2. EXPERIMENTAL

In this section we describe the DSA hole shrink sample fabrication followed by the TEM sample preparation as shown in Figure 1.

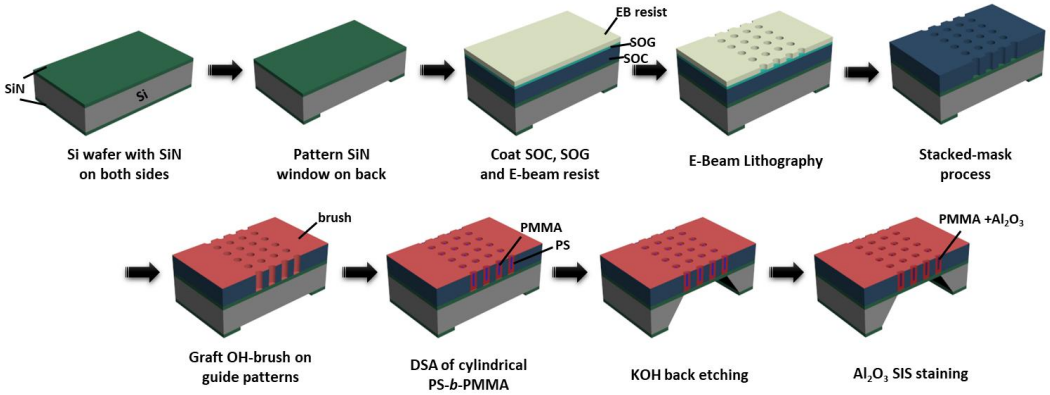

Figure 1. Schematic illustration of DSA process and TEM sample preparation.

2.1 Graphoepitaxy process flow

The templated DSA flow in this study is similar or same to what has been developed in imec.[12] The substrate was spin coated with ~100 nm of SOC and ~30 nm of SOG and ~60 nm of e-beam resist. E-beam lithography was performed to write hole patterns with ~55 nm in diameter and 110 nm pitch. The hole patterns were transferred from resist layer into the SOG and then from SOG to SOC through dry etch using CF_4 and O_2 gas RIE respectively. The SOG was removed by buffered oxidant etchant. Brush TOK1 or TOK2 were applied by spin-coating from solution (TOK-CDN024L or TOK-CDN022L), annealing at 280 °C for 1 min and removing ungrafted brush molecule by organic solvent rinse. The cylinder-forming PS-*b*-PMMA (TOK-CDB004L, center-to-center periodicity L_0 = 38 nm) was spin coated on the templates to a film thickness of approximately 20 nm (as measured from a similarly cast film on bare silicon) and annealed at 250 °C for 1 min under a N_2 environment. The DSA samples made from 300 mm track-processed wafer was prepared in imec, using photolithography and different brush and BCP materials as described in literature.[13]

2.2 TEM sample preparation

The aforementioned DSA hole shrink samples were prepared on the front side of a 200 µm thick Si wafer with 30 nm low-stress silicon nitride (SiN_x) deposited on double sides, and were made into TEM membrane sample using the methods as reported in an earlier paper.[10] SiN_x on the back side of wafer was patterned by optical lithography as the first step (Figure 1). After performing hole shrink DSA on the front side, wafers were back etched in KOH solution with front side sealed and protected to make several 3 mm × 3 mm TEM samples with target pattern area on the center of 1 mm × 200 µm large SiN_x windows for TEM imaging. The 300 mm track-processed was made into TEM samples using same approach, except the Si wafer thickness is 800 µm and the SiN_x film thickness is 15 nm.

2.3 STEM tomography and 3D reconstruction

We use the similar sample staining and STEM tomography steps as described in an earlier paper.[11,14] Al_2O_3 sequential infiltration synthesis (SIS) was performed on each TEM samples using alternating exposures to trimethylaluminum

(TMA) and deionized H_2O to selectively stain PMMA and provide imaging contrast and stability. STEM tomography was performed using a field-emission gun TEM (FEI Tecnai) operated at 200 kV. The camera length is 300 mm and samples were imaged using high angle annular dark field detector. Images were collected from hole shrink samples made on 200 μm thick Si wafer with holder tilting from -70° to +70° with 2° or 3° angular interval and dynamic focus. The range of tilting angles of 800 μm thick samples was narrowed down to about -54° to +54°. The tilt series were then aligned and reconstructed using Inspect3D software.

Segmentation (thresholding) of the reconstructed volume was performed using ImageJ. Binary signals corresponding to stained PMMA domains and SOC templates were separated into two stacks. The stack of PS domains was generated by filling the space between PMMA and SOC templates. The rendered 3D structure was visualized in software tomviz by displaying the contours of PMMA stack colored in blue and PS stack colored in red simultaneously**.**

2.4 Simulation

The simulation results presented in this work are based on the standard theoretically informed coarse-grained model,[15–17] which represents n block copolymer Gaussian chains discretized into N beads connected by harmonic springs in a fixed volume V at a fixed temperature T. This model has previously been shown to be in quantitative with experimental results.[18,19] In this model, the energy associated with the polymer bonds is a harmonic restraint, penalizing bonds from stretching or compressing away from their equilibrium value. The energy associated with non-bonded interactions is a combination of a Flory-Huggins type penalty governing the incompatibility of the two blocks (parametrized by the Flory-Huggins parameter χN) and a term enforcing a finite melt compressibility (parametrized by κ, related to the isothermal compressibility). The cylindrical confinement is imposed by hard walls; the sidewall and bottom substrate interact with the polymer according to a term parametrized by a proportionality constant Λ, the magnitude of which dictates the strength of substrate interactions, and the sign of which dictates preference for beads of type A or B. The model is implemented in the context of a Monte Carlo simulation. Configurations are sampled according to the Metropolis criterion; trial configurations are proposed using two different Monte Carlo moves; single bead displacement and chain reptation. Full mathematical details are available in the reference cited above.

3. RESULTS AND DISCUSSION

3.1 3D metrology for DSA hole shrink process

The direct observation of three-dimensional morphologies of PS-*b*-PMMA cylinders within templated holes is rarely reported mainly due to the challenges of sample preparation. Several studies used cross-sectional TEM to measure the amount of residual PS layer between PMMA cylinder and the bottom of templates.[6,8] However, as a destructive method, shrinkage and mismatch of thickness is often found as the issue. Okabe K *et al.* used FIB Pt deposition and milling to prepare cross-sectional TEM sample preparation. Using elemental mapping and 3D reconstruction, they successfully captured a noticeable amount of PS residual layer under the Pt filling.[6] Although FIB is versatile to make site-specific TEM samples, it requires the removal of material, and protecting polymers from FIB damage could be difficult. A reduction in SOG and SOC thickness as large as 40 nm was observed implying the potential compression of BCP structure as well, which greatly affects the accuracy of their measurement.[6] Therefore, it is important to develop a more nondestructive approach to characterize DSA hole shrink process in three dimensions. Dixit D *et al*. reported that they used a ellipsometry-based scatterometry to optically characterize DSA hole shrink samples, which can nondestructively predict dimensional changes.[20] However, this method is limited to characterize DSA-induced defects, and without comparison with 3D real space information it is difficult to evaluate the accuracy of their applied optical model.

Recently, STEM tomography has been used to probe different BCP 3D structures and it is especially suitable for capture heterogeneous and complicated morphologies.[11,14,21] Using an established TEM sample preparation approach based on back etching of SiN_x coated <100> Si wafer[10], the template made of SOC as well as block polymer films on the front side of wafer could be perfectly preserved. Using SIS staining, the shape of polymer interface could be clearly revealed, which avoids any potential modifications caused by selective removal of polymer domain and metal deposition. Although the field of view in STEM tomography is limited (1 μm ×1 μm in this study) in order to get high resolution images, the 3D volume of about thirty holes could be captured in each tomography series which offers a much larger field of view than regular cross-sectional images and more representative and statistical data. With all these advantages,

the 3D metrology used in this study could be a high throughput method to acquire the detailed information of DSA hole shrink process in all dimensions.

3.2 Effects of surface chemistry

Previous simulation studies have predicted that both the surface chemistry and geometry of cylindrical templates play important role in guiding the DSA of BCP cylinders.[8,9] In terms of surface chemistry, ideally perfect DSA is achieved when sidewall is wetting to PS and bottom is non-preferential to PS and PMMA.[8,9] The challenge to reach this ideal situation is that, during SOC etch step both sidewall and bottom surface are exposed to oxygen-containing plasma and that both could be easily modified by OH terminated polymer brush. There is difference in materials though: the surface of sidewall is plasma exposed SOC and the surface of bottom is plasma exposed SiN_x (or other substrates). Doise J *et al.* developed a dual-brush process which independently modify the sidewall and bottom surface by consecutively grafting two brushes with distinct end-groups.[13] In our study of surface chemistry effects, only one brush was used in each DSA sample, but the surface chemistry was controlled by kinetically grafting of the brush. Two OH terminated polymer brush (different monomer) was found that when grafting at high temperature they could modify the sidewall and bottom surface differently (Table 1). The TOK1 brush makes both sidewall and bottom surface PS-preferential, while TOK2 brush makes sidewall surface preferential to PS block and bottom surface non-preferential to PS and PMMA blocks. Two DSA samples was made on SiN_x membrane for TEM characterization with sample DSA procedure except using TOK1 or TOK2 to modify the surface of template. There is no significant difference in this two samples in SEM as both of them showing successful DSA singlets from top down. However, the STEM tomography revealed more distinct cylinders structures between these two samples.

Table 2. Schematic illustration of sample preparation for 3D characterization

Brush	SOC sidewall	SiN_x Bottom
TOK-CDN024L (TOK1)	PS-preferential	PS-preferential
TOK-CDN022L (TOK2)	PS-preferential	non-preferential

Figure 2 shows the reconstruction results of the two samples. For each sample, three *xy* slices (parallel to the substrate) displaying 4 × 4 DSA holes were taken from different heights *z* of the reconstruction volume where $z = 0$ is defined as the height of bottom of prepatterned holes (or top surface of SiN_x). The bright domain inside of each hole corresponds to the Al_2O_3-stained PMMA cylinder domain while the outer bright domain corresponds to the Al_2O_3-stained outline of SOC template. The staining effect of the sidewall surface may result from polar components generated on the plasma exposed area during SOC etch. The 3D visualization was done on one DSA hole on each sample where the Al_2O_3-stained PMMA block is colored in blue and the PS block is colored in red.

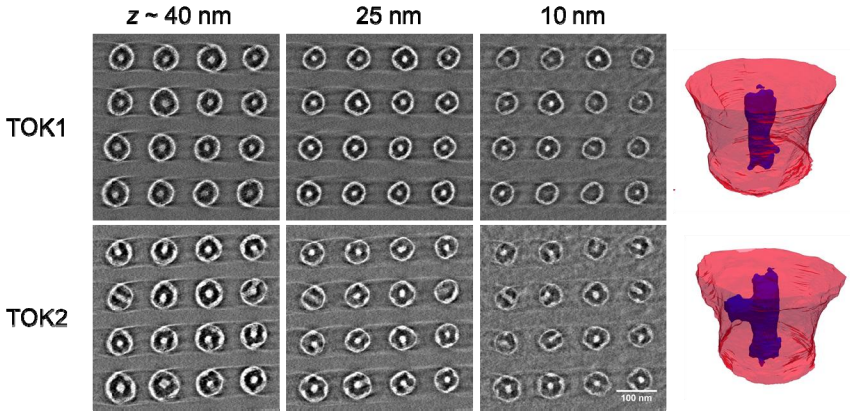

Figure 2. Tomography reconstruction results of two DSA samples using different brush. *xy* slices were taken at different sample height. The brighter domains are Al_2O_3-stained PMMA or the sidewall surface and the darker domains are PS and SOC template. In the 3D visualization, Al_2O_3-stained PMMA is in blue color and PS is in red color.

For the DSA sample using brush TOK1, all PMMA cylinders are at about the center of the template without connecting to sidewall from top to bottom. In the slice at z = 10 nm which is close to bottom substrate, only about seven out of sixteen holes still show signal from well-defined PMMA cylinders, which indicates the existence of PS residual layer in the bottom of about 50% of DSA holes. As for the other DSA samples using brush TOK2, the morphologies are distinct through BCP thickness. At in the slice taken at z = 40 nm where it is slightly beneath the BCP top surface, most of the PMMA cylinders are still relative close to the center of template while few of them start showing irregular shape and connecting to sidewalls. At z = 25 nm where it is relatively at the height of half of filled BCP thickness, the bridging to sidewall could be found in most of DSA holes. When z = 10 nm, the cylinder domains are still very distorted, but all the holes still have signal from PMMA. This height evolution shows that the TOK2 sample having more distorted PMMA cylinders which have many bridge-like defects connecting to SOC sidewall, but all PMMA cylinders reach to bottom substrates and there is much less PS residual defects. The 3D rendering shows the representative DSA results of each brush: the TOK1 gives vertical cylinder domain; the TOK2 gives bridging defects connecting to sidewall.

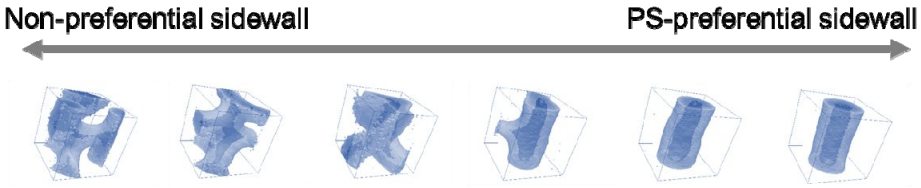

Figure 3. Simulation results using coarse-grained model where the volume franction of PMMA is 0.3 and the diameter of confinement is 50 nm (1.32 L_0). Only the PMMA block is presented in blue color.

The fact that DSA sample using brush TOK1 has more PS residue defects could be attributed to PS-preferential bottom surface. For TOK2, its non-preferential bottom surface leads to through-film PMMA domains in majority. However, the existence of bridging to sidewalls indicates the wetting behavior of TOK2 modified sidewall is different. In ideal DSA singlet, the area fraction of PS (f_{PS}) at the sidewall interface should be 100% if the sidewall surface exactly likes PS. The bridging defects happen when f_{PS} needs to be decreased to reach minimum interfacial free energy, which implies that the preferentiality of modified sidewall surface to PS decreased.

To better understand which surface behavior leads to the bridging defects, coarse-grained model is used to simulate the DSA results in cylindrical confinement with non-preferential bottom and altering attraction of sidewall to PS as shown in Figure 3. When the sidewall surface is changing from strongly PS-preferential to non-preferential, it is predicted that the morphology of PMMA will change from a vertical cylinder domain in the center to an expanded and distorted shape with increasing contact area to sidewall. In the middle point where the sidewall surface is slightly PS-preferential, the simulated morphology has vertical cylinder with bridging defect reaching to sidewall, which is similar with our experimental observations of TOK2 sample.

Comparing the 3D structure of DSA samples observed from tomography to the simulated morphology, a more precise description of the surface properties of those two samples would be: TOK1 makes both sidewall and bottom surface strongly PS-preferential; TOK2 makes the bottom non-preferential and the sidewall only slightly PS-preferential. It is highly possible that, when trying to reach non-preferential bottom using a single-brush process, the attraction of sidewall to PS is often sacrificed. When simulation studies encourage to use non-preferential bottom surface to eliminate PS residual layer, it is worth noting that the surface chemistry of sidewall is crucial as well. It is necessary to keep sidewall surface in the strongly PS preferential region to avoid any distortion of vertical PMMA cylinders.

3.3 Effects of geometry

The geometry of graphoepitaxial template also has great impact on the DSA results. The diameter of template must match the periodicity of BCP to form singlets, and when sidewall wets the majority block the critical dimension (CD) required is around one times the pitch of BCP.[22] Considering the thickness of brush grafted to template surface, the CD is often slightly larger than the pitch of BCP and with certain tolerance judged from the hole open yield.[4,23] The matching between BCP periodicity and CD of template is considered very important as holes too small or too large could result in more PS residual layer in the bottom and missing holes after pattern transfer.[4] Here we probe several DSA pattern area with different template size using STEM tomography to better understand how the template size affect the quality of DSA in more dimensions.

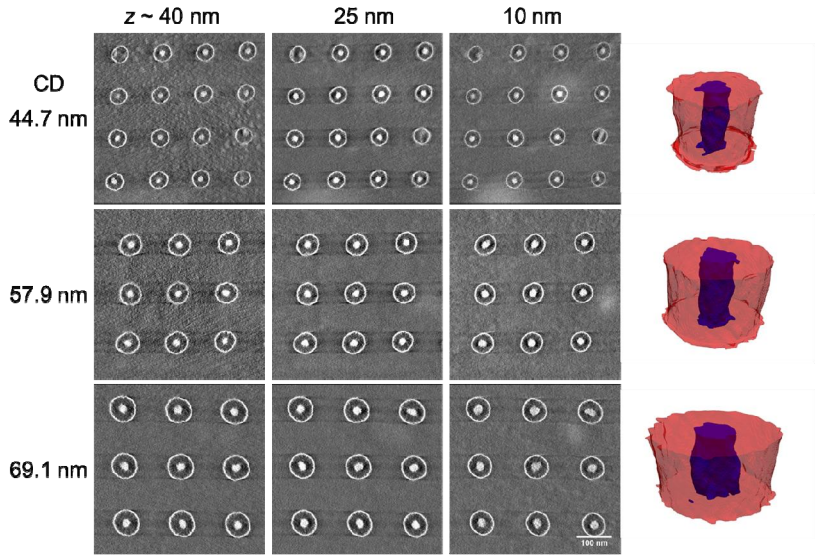

Figure 4. Tomography results of singlets with different template CD

Figure 4 shows the tomography results of three DSA area with CD of template of 44.7 nm, 57.9 nm and 69.1 nm (as measured from TEM image). As this TEM sample is prepared from 800 µm thick track-processed wafer, the wafer thickness limits the maxium tilting angle in tomogrpahy series to 54°, but the reconstruction results are still of good quality and high resolution. These DSA patterns were made through dual-brush process amd the reported CD process window for wafer prepared through same DSA conditions is about 47-58 nm.[13] The three pattern area selected has CD smaller than this window, in the window and larger than the window respectively. Again, *xy* slices were taken at three different sample height: close to top of the film at $z \sim 40$ nm, middle of the film at $z \sim 25$ nm and relatively bottom of the film at $z \sim 10$ nm. For all three DSA pattern, PS-residule layer is not observed and the signal from PMMA cylinders is still very clear even in the bottom of the film. In the template with CD of 44.7 nm, two out of sixteen DSA holes are defective without well-defined vertical cylinders. When CD is 57.9 nm, all three *xy* slices look very similar indicates the DSA cylinders are in circular shape and very uniform thoughut the thickness. At the largest CD (69.1 nm), most of the DSA cylinders are circular but we notice some cylinders start to show more irregular shape. For example, the hole in the top right corner is in more oval shape.

These observation verifies that, even when the CD of template is outside of optimized process window, the dual-brush process successfully prevents the formation of PS-residual layer in the bottom. Comparing with the single brush process used in the surface chemistry study, the dual-brush process is more effective to control the sidewall and bottom surface separatly and leads to better DSA quality. We also found, when the CD is smaller than the process window, there isn't obsious PS residual layer in the bottom. However, there is more dramastic change in the DSA morphology and in some holes the vertical cylinder can't even form, which could be the real cause to the missing singlets after pattern tranfer. When is CD is slightly larger than the process window, some cylinders become slightly distorted and if it happens in most of the film thickness the distortion could be etched into underlying substrate and makes pattern transfer not ideal.

4. SUMMARY

In our study, the DSA hole shrink samples are prepared on SiN_x membrane in a non-destructive way and characterized in three dimensions with STEM tomography. Different DSA structures are revealed when the e-beam patterned template is modified differently. Confirmed with simulation study, bridging defects connecting the PMMA cylinder with sidewall will show up when the sidewall surface is changed from being strongly to weakly PS-preferential. It is thus important to make sure the attraction of sidewall to PS is still strong enough when trying to make bottom surface non-preferential, which might be more difficult to achieve for single brush process compared to dual-brush process. Singlet DSA hole shrink sample with different template CD sizes was prepared from track-processed wafer and characterized using

tomography in a similar approach. Based on the obtained 3D information, it is found that the dual-brush process could effectively avoid PS-residual in the bottom over a wide CD range. And several types of DSA defects were identified as potential attributors to observed pattern transfer defects when CD is outside of the process window. This study captures different defective DSA structures happening in templates with different surface chemistry and geometry, which greatly helps to develop a fundamental understanding of the key DSA factors for optimization of the hole shrink process.

ACKNOWLEDGEMENTS

This work was supported in part by Semiconductor Research Corporation (SRC) and Tokyo Ohka Kogyo Co., Ltd. (Japan). C. Z. is a graduate student supported by SRC. Use of the Center for Nanoscale Materials, an Office of Science user facility, was supported by the U.S. Department of Energy, Office of Science, Office of Basic Energy Sciences, under Contract No. DE-AC02-06CH11357. We thank Dr. Leonidas E. Ocola and Dr. Nestor J. Zaluzec for helpful discussion. This work made use of the Pritzker Nanofabrication Facility of the Institute for Molecular Engineering at the University of Chicago, which receives support from Soft and Hybrid Nanotechnology Experimental (SHyNE) Resource (NSF ECCS-1542205), a node of the National Science Foundation's National Nanotechnology Coordinated Infrastructure.

REFERENCES

[1] Ruiz, R., Kang, H., Detcheverry, F. A., Dobisz, E., Kercher, D. S., Albrecht, T. R., De Pablo, J. J. and Nealey, P. F., "Density multiplication and improved lithography by directed block copolymer assembly," Science **321**(5891), 936-939 (2008).

[2] Jeong, S. J., Kim, J. Y., Kim, B. H., Moon, H. S. and Kim, S. O., "Directed self-assembly of block copolymers for next generation nanolithography," Mater. Today **16**(12), 468-476 (2013).

[3] Yi, H., Bao, X. Y., Zhang, J., Bencher, C., Chang, L. W., Chen, X., Tiberio, R., Conway, J., Dai, H., Chen, Y., Mitra, S. and Wong, H. S. P., "Flexible control of block copolymer directed self-assembly using small, topographical templates: Potential lithography solution for integrated circuit contact hole patterning," Adv. Mater. **24**(23), 3107-3114 (2012).

[4] Seino, Y., Yonemitsu, H., Sato, H., Kanno, M., Kato, H., Kobayashi, K., Kawanishi, A., Azuma, T., Muramatsu, M., Nagahara, S., Kitano, T. and Toshima, T., "Contact hole shrink process using graphoepitaxial directed self-assembly lithography," J. Micro/Nanolithography, MEMS, MOEMS **12**(3), 033011-033011 (2013).

[5] Gharbi, A., Tiron, R., Argoud, M., Chevalier, X., Barros, P. P., Nicolet, C. and Navarro, C., "Contact holes patterning by directed self-assembly of block copolymers: process window study," J. Micro/Nanolithography, MEMS, MOEMS **14**(2), 023508-023508 (2015).

[6] Okabe, K., Yi, H., Tung, M. C., Tiberio, R., Bekaert, J. and Gronheid, R., "Cross-Sectional Imaging of Directed Self Assembled Block Copolymers," SPIE **9423**, 1-9 (2015).

[7] Iwama, T., Laachi, N., Delaney, K. T., Kim, B., Hur, S., Bristol, R., Shykind, D., Weinheimer, C. J. and Fredrickson, G. H., "The Hole Shrink Problem: Directed Self-Assembly Using Self-Consistent Field Theory," J. Photopolym. Sci. Technol. **26**(1), 15-20 (2013).

[8] Yoshimoto, K., Fukawatase, K., Ohshima, M., Naka, Y., Maeda, S., Tanaka, S., Morita, S., Aoyama, H. and Mimotogi, S., "Optimization of directed self-assembly hole shrink process with simplified model," J. Micro/Nanolithography, MEMS, MOEMS **13**(3), 31305 (2014).

[9] Peters, B. L., Rathsack, B., Somervell, M., Nakano, T., Schmid, G. and De Pablo, J. J., "Graphoepitaxial assembly of cylinder forming block copolymers in cylindrical holes," J. Polym. Sci. Part B Polym. Phys. **53**(6), 430-441 (2015).

[10] Ren, J., Ocola, L. E., Divan, R., Czaplewski, D. A., Segal-Peretz, T., Xiong, S., Kline, R. J., Arges, C. G. and Nealey, P. F., "Post-directed-self-assembly membrane fabrication for in situ analysis of block copolymer structures," Nanotechnology **27**(43), 435303 (2016).
[11] Segal-peretz, T., Zhou, C., Ren, J., Dazai, T., Ocola, L. E., Divan, R. N. S. and Nealey, P. F., "Three Dimensional Assembly in Directed Self-assembly of Block Copolymers," J. Photopolym. Sci. Technol. **29**(5), 653-657 (2016).
[12] Doise, J., Bekaert, J., Chan, B. T., Hori, M. and Gronheid, R., "Via patterning in the 7-nm node using immersion lithography and graphoepitaxy directed self-assembly," J. Micro/Nanolithography, MEMS, MOEMS **16**(2), 23506 (2017).
[13] Doise, J., Chan, B. T., Hori, M. and Gronheid, R., "Dual brush process for selective surface modification in graphoepitaxy directed self-assembly," 101460R (2017).
[14] Segal-Peretz, T., Winterstein, J., Doxastakis, M., Ramírez-Hernández, A., Biswas, M., Ren, J., Suh, H. S., Darling, S. B., Liddle, J. A., Elam, J. W., de Pablo, J. J., Zaluzec, N. J. and Nealey, P. F., "Characterizing the Three-Dimensional Structure of Block Copolymers via Sequential Infiltration Synthesis and Scanning Transmission Electron Tomography," ACS Nano **9**(5), 5333-5347 (2015).
[15] Matsen, M. W. and Schick, M., "Stable and Unstable Phases of a Linear Multiblock Copolymer Melt," Macromolecules **27**(24), 7157-7163 (1994).
[16] Fredrickson, G., [The Equilibrium Theory of Inhomogeneous Polymers] (2007).
[17] Detcheverry, F., Pike, D., Nealey, P., Müller, M. and De Pablo, J., "Monte Carlo Simulation of Coarse Grain Polymeric Systems," Phys. Rev. Lett. **102**, 2-5 (2009).
[18] Detcheverry, F. A., Kang, H., Daoulas, K. C., Müller, M., Nealey, P. F. and De Pablo, J. J., "Monte Carlo simulations of a coarse grain model for block copolymers and nanocomposites," Macromolecules **41**(13), 4989-5001 (2008).
[19] Detcheverry, F. A., Liu, G., Nealey, P. F. and De Pablo, J. J., "Interpolation in the directed assembly of block copolymers on nanopatterned substrates: Simulation and experiments," Macromolecules **43**(7), 3446-3454 (2010).
[20] Dixit, D., Green, A., Hosler, E. R., Kamineni, V., Preil, M. E., Keller, N., Race, J., Chun, J. S., O'Sullivan, M., Khare, P., Montgomery, W. and Diebold, A. C., "Optical critical dimension metrology for directed self-assembly assisted contact hole shrink," J. Micro/Nanolithography, MEMS, MOEMS **15**(1), 14004 (2016).
[21] Segal-Peretz, T., Ren, J., Xiong, S., Khaira, G., Bowen, A., Ocola, L. E., Divan, R., Doxastakis, M., Ferrier, N. J., De Pablo, J. and Nealey, P. F., "Quantitative Three-Dimensional Characterization of Block Copolymer Directed Self-Assembly on Combined Chemical and Topographical Prepatterned Templates," ACS Nano **11**(2), 1307-1319 (2017).
[22] Doise, J., Bekaert, J., Chan, B. T., Gronheid, R., Cao, Y., Hong, S., Lin, G., Fishman, D., Chakk, Y. and Marzook, T., "Implementation of surface energy modification in graphoepitaxy directed self-assembly for hole multiplication," J. Vac. Sci. Technol. B, Nanotechnol. Microelectron. Mater. Process. Meas. Phenom. **33**(6), 06F301 (2015).
[23] Delgadillo, P. A. R., "Implementation of a chemo-epitaxy flow for directed self-assembly on 300-mm wafer processing equipment," J. Micro/Nanolithography, MEMS, MOEMS **11**(3), 31302 (2012).